An experimental and computational study of donor-linker-acceptor block copolymers for organic photovoltaics

Zhiqi Hu[1], Jacek Jakowski[2,3], Chenyu Zheng[4], Christopher J. Collison[4], Joseph Strzalka[5], Bobby G. Sumpter[2], R. Verduzco[1,6]

[1]Department of Chemical and Biomolecular Engineering, Rice University, 6100 Main Street, MS-362, Houston, TX 77005 USA

[2]Center for Nanophase Materials Sciences, Oak Ridge National Laboratory, 9500 Spallation Drive, Oak Ridge, TN 37830 USA

[3]Computer Science and Mathematics Division, Oak Ridge National Laboratory, 9500 Spallation Drive, Oak Ridge, TN 37830 USA

[4]School of Chemistry and Materials Sciences, Rochester Institute of Technology, 84 Lomb Memorial Drive, 08-3290 Gosnell, NY 14623 USA

[5] X-ray Science Division, Argonne National Laboratory, 9700 South Cass Avenue, Argonne, IL 60439

[6]Department of Materials Science and NanoEngineering, Rice University, 6100 Main Street, MS-325, Houston, TX 77005 USA

Correspondence to: Rafael Verduzco (E-mail: *rafaelv@rice.edu*)

Additional Supporting Information may be found in the online version of this article.

ABSTRACT

Block copolymers with donor and acceptor conjugated polymer blocks provide an approach to dictating the donor-accepter interfacial structure and understanding its relationship to charge separation and photovoltaic performance. We report the preparation of a series of donor-linker-acceptor block copolymers with poly(3-hexylthiophene) (P3HT) donor blocks, poly((9,9-dioctylfluorene)-2,7-diyl-alt-[4,7-bis(thiophen-5-yl)-2,1,3-benzothiadiazole]-2′,2″-diyl) (PFTBT) acceptor blocks, and varying lengths of oligo-ethylene glycol (OEG) chains as the linkers. Morphological analysis shows that the linkers increase polymer crystallinity while a combination of optical and photovoltaic measurements show that the insertion of a flexible spacer reduces fluorescence quenching and photovoltaic efficiencies of solution processed photovoltaic devices. Density functional theory (DFT) simulations indicate that the linking groups reduce both charge separation and recombination rates, and block copolymers with flexible linkers will likely rotate to assume a non-planar orientation, resulting in a significant loss of overlap at the donor-linker-acceptor interface. This work provides a systematic study of the role of linker length on the photovoltaic performance of donor-linker-acceptor block copolymers and indicates that linkers should be designed to control both the electronic properties and relative orientations of conjugated polymers at the interface.

KEYWORDS: block copolymers, organic photovoltaics, linking groups, donor, acceptor

INTRODUCTION

Organic photovoltaics (OPVs) are attractive alternatives to crystalline silicon and other inorganic photovoltaics due to their low weight and cost, favorable processing characteristics, and mechanical flexibility.[1–3] Recent work has demonstrated large-scale printable OPV installations,[4] and a favorable levelized cost of energy for OPV modules compared to inorganic photovoltaics.[5] State-of-the-art OPVs consist of a blend of donor and acceptor organic semiconductors, and controlling the morphology of the blend is a persistent challenge.[6–10] An important aspect of the morphology that has a large impact on photovoltaic performance is the structure and composition at the donor-acceptor interface. Unlike inorganic photovoltaics, absorption of light in OPVs results in the formation of a bound electron-hole pair known as an exciton which can undergo a charge separation process to produce free charges. The structure of the donor-acceptor interface is crucial for efficient charge separation, but a firm understanding of the optimal structure and composition of the donor-acceptor interface to promote charge separation is lacking.[11,12] Further, rational strategies to modify the donor-acceptor interface to promote more efficient charge separation are limited.

Recent studies have determined important characteristics of the donor-acceptor interface that can influence charge transfer. For example, Shaw et al. measured a drop in energy transfer kinetics for donor/spacer/acceptor multilayer films with increasing spacer thickness,[13] and Zhong et al. found an enhancement in photovoltaic performance when a thin insulating spacer was introduced between donor and acceptor layers.[14] Strategies have been developed in bulk heterojunction devices where additives that segregate to the donor-acceptor interface can serve as insulating spacers that suppress interfacial recombination processes.[15,16] These studies demonstrate that introducing a thin, insulating spacer between donor and acceptor domains can be beneficial to photovoltaic performance. Density functional theory simulations predict a significant suppression of interfacial charge recombination with sharp interfacial domains.[17]

All-conjugated block copolymers (BCPs) which consist of covalently-bound donor and acceptor polymers provide a potential alternative for studying charge separation and recombination processes at the donor-acceptor interface. These materials have been implemented in single-component photovoltaic devices, as detailed in recent publications[7,10,18-21] In our previous work, we also showed that the composition of the linking group between donor and acceptor domains can play a critical role in charge separation.[22] However, a systematic study of the role of the linking group in all-conjugated BCPs with a flexible, insulating linker has not been carried out, and only a few prior studies have reported all-conjugated BCPs with flexible linkers.[23–25]

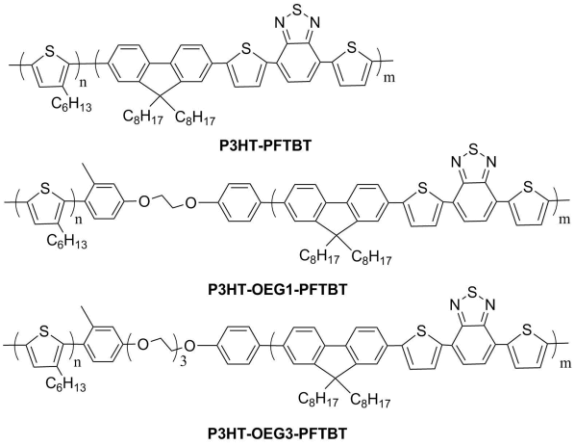

FIGURE 1. All-conjugated BCPs with varying linking group length reported in this study. P3HT serves as the donor, PFTBT as the acceptor, and OEG as the insulating linking group.

In this work, we present an approach to make a series of BCPs while introducing a variable but controlled length flexible linking group between the conjugated donor and acceptor blocks. We furthermore carry out comprehensive optical

and photovoltaic performance analysis of our materials along with computational studies of the impact of the flexible linking group on charge transfer processes. This study provides insight into the structure and properties of linking groups for BCP OPVs and indicates that a short, rigid insulator is expected to be superior to flexible linking groups for photovoltaic applications.

EXPERIMENTAL

Materials. All reagents and starting materials were purchased from commercial sources and used as received. 2,5-dibromo-4-hexyl thiolphene[26], P3HT-Br (M_n = 8.5 kDa, $Đ$ = 1.36) and P3HT-PFTBT (M_n = 14.6 kDa, $Đ$ = 2.09)[27] was synthesized as previously described. Details on the preparation of 2-(4-chloro-3-methylphenol) ethanol, 2-(4-chloro-3-methylphenol) ethanol tosylate, Ditosyl-triethylene glycol, 2-(4-chloro-3-methylphenol) triethylene glycol tosylate, 2-(4-chloro-methylphenol) ethanol tosylate end functionalized poly(3- hexylthiophene), (P3HT-OEG1Ts), 4-bromophenol ethylene glycol end functionalized poly(3-hexylthiophene) (5), Poly(3-hexylthiophene)-b-2-(4-chloro-methyl phenol) ethanol-b-(9′,9′,-dioctylfluorene)-b-oligo(2,7-(9′,9′,–dioctylfluorene)-alt-5,5-(4′,7′-di-2-thienyl-2′,1′,3′,-benzothiadiazole) (P3HT-OEG1-PFTBT), 2-(4-chloro-methylphenol) triethylene glycol tosylate end functionalized poly(3-hexylthiophene), (P3HT-OEG3Ts), 4-bromophenol triethylene glycol end functionalized poly(3-hexylthiophene) (6), and Poly(3-hexylthiophene)-b-2-(4-chloro-methylphenol) triethanol-b-(9′,9′,-dioctylfluorene)-b-poly(2,7-(9′,9′,-dioctylfluorene)-alt-5,5-(4′,7′-di-2-thienyl-2′,1, 3′,-benzothiadiazole) (P3HT-OEG3-PFTBT) are presented in the supporting information. 1H NMR spectroscopy for all materials are presented in the Supporting Information Figures S1 – 11.

INSTRUMENTATION

Gel permeation chromatography (GPC): Gel permeation chromatography (GPC) was carried out to determine molecular weight (M_n) and moleculwar weight dispersity ($Đ$) for each polymer. The GPC system is equipped with differential refractive index (RI) and UV-Vis absorbance spectrometer. Tetrahydrofuran (THF) was used as the mobile phase for GPC with flow rate of 1 mL/min. M_n and $Đ$ were determined relative to polystyrene standards.

Nuclear Magnetic Resonance Spectroscopy (NMR): Measurements were carried out with a Bruker 400 MHz. Samples were prepared at 10 mg/mL concentration. The solvent contains chloroform with 0.05% TMS.

Ultraviolet-visible absorption (UV-Vis): UV-Vis measurements were carried out with a Shimadzu UV 2550. The absorbance wavelength was acquired in the range from 350 nm to 750 nm.

Steady-state photoluminescence (PL): PL measurements were carried out with a Horiba FluoroLog-3 spectrofluorometer. The excitation wavelength was fixed at 470 nm, and absorbance and PL spectra were normalized with respect to their maximum intensity. For PL quenching measurements, the PL intensity was normalized with respect to the absorbance intensity at 470 nm.

Grazing Incidence Wide-Angle X-ray Scattering (GIWAXS): Measurements were carried out on Beamline 8-ID-E at the Advance Photon Source, Argonne National Laboratory. The photon energy was fixed at 10.92 eV. The specimen detector distance was 228 mm, and incident angle was 0.14°.

Fabrication and testing of photovoltaic devices: Photovoltaic devices consisted of an inverted architecture of ITO/ZnO/active layer/PEDOT: PSS/Ag. The active layer was composed of pure block copolymer or block copolymer mixed with P3HT and PCBM at a fixed mass ratio of 0.6:1:1. The overall concentration of the active layer solution before spin-casting was 20 mg/ml in chlorobenzene. The solution was stirred for 12

hr before use. The ZnO precursor solution was prepared by dissolving 1 g of zinc acetate dehydrate in 10mL of 2-methoxyethanol with 0.28 g of ethanolamine as a surfactant. The PEDOT: PSS solution was prepared by diluting l mL of PEDOT:PSS Clevios P VP AI 4083 (Heraeus) in 10 mL isopropanol. ITO glass was cleaned sequentially for 15 min in ultrasonic baths using deionized soap water (0.5% Hellmanex III, Helma), deionized water, acetone, and isopropanol, and dried in an oven at 90 °C for 1 hr. The ITO glass was treated with UV-ozone before coating the ZnO precursor. The ZnO precursor was spin-coated onto the ITO glass at 2000 rpm for 1 min, and thermally annealed at 200 °C for 1 hr. The substrate was then rinsed with acetone and isopropanol, and dried in an oven at 90 °C for 1 hr. The substrate was then transferred to a nitrogen-filled glovebox. Active layer was then spin-coated on top of ZnO layer at 800 rpm for 1 min and annealed for 15 min at 165 °C. The substrate was cooled to room temperature, and was spin-coated at 5000 rpm for 1.5 min. A silver anode was deposited through a shadow mask under vacuum by thermal deposition to get a 200 nm thick layer. J-V curve was measured using a Keithley source measure unit. The solar cell performance was measured with a Newport AM 1.5 G solar simulator at an irradiation power of 310 W.

RESULTS AND DISCUSSION

Our target materials consisted of block copolymers (BCPs) with P3HT as the donor block, PFTBT as the acceptor block, and different linking groups between the two blocks, as shown in **Figure 1**. While we and others have previously studied this block copolymer system,[22,27–29] a method to introduce a flexible, insulating linker between donor and acceptor polymer blocks has not been reported. The block copolymer P3HT-PFTBT with no flexible linker between donor and acceptor polymer blocks was synthesized as previously reported, using a combination of Grignard metathesis (GRIM) to synthesize functionalized P3HT macromonomer followed by Suzuki-Miyaura polycondensation to attach the acceptor polymer block[27,30,31].Our synthetic strategy for introducing a flexible linker between donor and acceptor polymer blocks took advantage of chemistries for end-functionalization of P3HT using an externally initiated polymerization[32–36] and is shown in **Schemes 1 and 2**. A functionalized initiator was first synthesized by reacting 2-(4-chloro-3-methylphenol) ethanol tosylate or 2-(4-chloro-3-methylphenol)-triethyl glycol tosylate with $Ni(PPh_3)_4$ followed by ligand exchange with dppp.[32] The resulting initiator was used in the synthesis of P3HT through GRIM, followed by modification of the tosylate endgroup to introduce aryl bromide functionality. Next, the PFTBT block was synthesized by Suzuki-Miyaura polycondensation, resulting in all-conjugated block copolymers with flexible linking groups between donor and acceptor blocks.

^{1}H NMR provides direct evidence for the attachment of the OEG linking groups to P3HT. For both P3HT macromonomers, ^{1}H NMR peaks corresponding to the oligoethylene glycol endgroup are clearly resolved. For P3HT-OEG1Ts, two distinct peaks at δ (ppm) = 4.16 and δ (ppm) = 4.38 corresponds to the $–CH_2$ groups on OEG1 after Grignard reaction (**Figure S5**). For P3HT-OEG3Ts polymer, a total of 6 $–CH_2$ groups in OEG3 correspond to NMR peaks ranging between 3.6-4.16 ppm (**Figure S8**). Linking groups attached to the final block copolymers can also be resolved by ^{1}H NMR, as shown in **Figures S7, S10, and S11.**

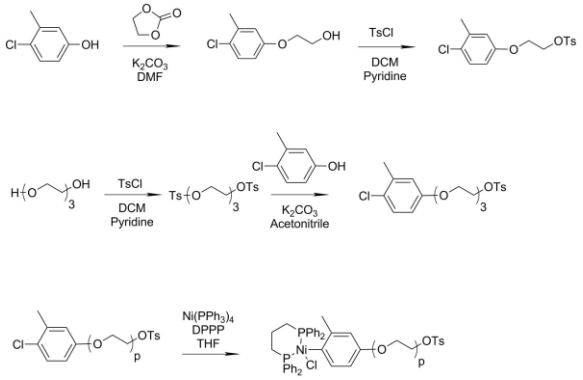

SCHEME 1. Schematic synthesis for functionalized Ni catalyst, the length of linking group p is 1 for OEG1 and 3 for OEG3

GPC provides evidence for successful preparation of target block copolymers, as reflected in a clear shift in the molecular weight distribution for the final block copolymer relative to the P3HT macromonomer. GPC data with both RI and UV-VIS analysis is presented in the Supporting Information (**Figures S12-17**). The UV-Vis analysis can distinguish between P3HT and PFTBT blocks, with a detection wavelength of 450 nm corresponding to the peak absorbance of P3HT. A shift in the peak absorbance for the final block copolymers relative to P3HT homopolymers (**Figures S15-17**) indicates successful attachment of PFTBT and formation of block copolymer.

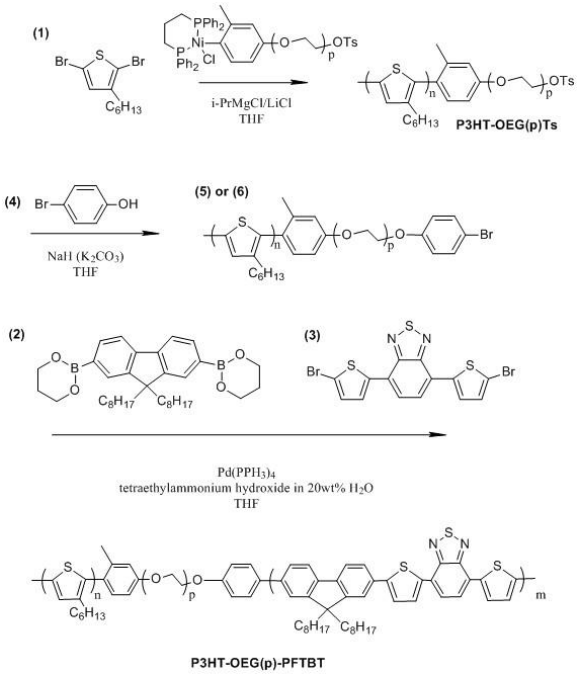

SCHEME 2. Schematic synthesis for block copolymer P3HT-PFTBT with flexible OEG linking group. The length of the linking group p is 1 for P3HT-OEG1-PFTBT and 3 for P3HT-OEG3-PFTBT

The morphology and crystallinity for each BCP and corresponding ternary blend was analyzed by grazing incidence wide-angle x-ray scattering (GIWAXS). The P3HT lamellar stacking corresponds to peak at q = 0.4 Å^{-1}. As seen in **Figure S18-21**, a significant increase in peak intensity for P3HT lamellar stacking is observed seen with increase length of linking group. This indicates that insertion of a flexible linking group increases the P3HT crystallinity, likely due to increased flexibility at the block copolymer junction. A similar result was found in a study by Lee et al. along with improved photovoltaic performance.[25]

TABLE 1. Number-averaged molecular weight M_n, molecular weight dispersity $Đ$, and mass fraction for each block copolymer

Block Copolymer	M_n (kDa)	$Đ$	P3HT content (wt %)[a]
P3HT-PFTBT	14.6	2.09	58
P3HT-OEG1-PFTBT	16.2	1.88	61
P3HT-OEG3-PFTBT	14.9	3.33	67

[a] P3HT wt % determined by GPC from the M_n of P3HT and its corresponding block copolymer

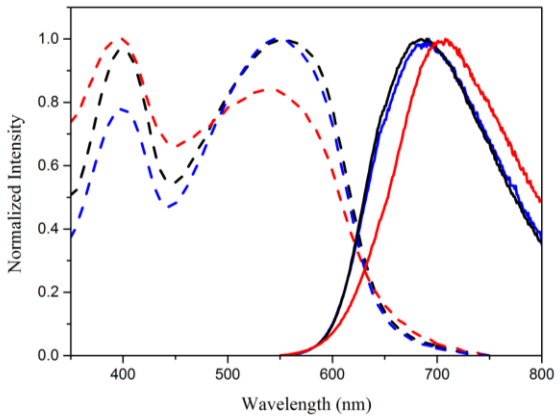

FIGURE 2. Normalized absorbance (dash lines) and photoluminescence (solid lines) for P3HT-PFTBT (black), P3HT-OEG1-PFTBT (blue) and P3HT-OEG3-PFTBT (red). Absorbance and PL spectra were normalized with respect to their maximum intensity.

To understand the impact of the flexible linker on electronic and optical properties, absorbance and photoluminescence spectra were acquired. Compared to P3HT-PFTBT, there is a small redshift of the PL peak for P3HT-OEG1-PFTBT polymer and a larger redshift for P3HT-OEG3-PFTBT. In prior work from our group where we compared the optical properties of P3HT-PFTBT differing in the composition of the linker, we observed a similar shift of the PL emission maximum with varying linker composition.[22] The redshift in the PL intensity is weaker for the present samples, but similarly reflects an impact of the linking group composition on the energetics at the donor-acceptor interface. This is also supported through density functional theory (DFT) calculations described below.

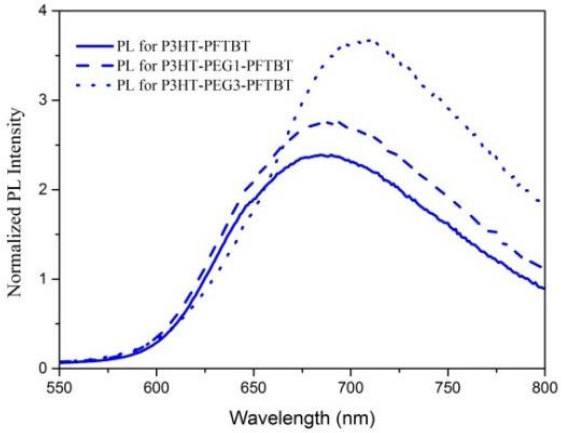

FIGURE 3. Photoluminescence (PL) quenching for P3HT-PFTBT, P3HT-OEG1-PFTBT and P3HT-OEG3-PFTBT with excitation at 470 nm and normalized by the absorbance at 470 nm.

Energy and charge transfer processes at the interface were probed through photoluminescence quenching measurements. Block copolymers at a concentration of 2 mg/ml in chlorobenzene were spin-cast on a glass substrate, and photoluminescence data for each block copolymer were acquired at a fixed excitation wavelength of 470 nm and normalized with respect to the absorbance at that same wavelength, as shown in **Figure 3**. PL for pure P3HT, PFTBT, and ternary blend are shown in Figure S22 – 24. A clear trend is observed where block copolymers with shorter linking groups exhibit stronger quenching of the normalized photoluminescence intensity. This suggests that the incorporation of linking groups reduces energy and charge transfer processes at the interface.

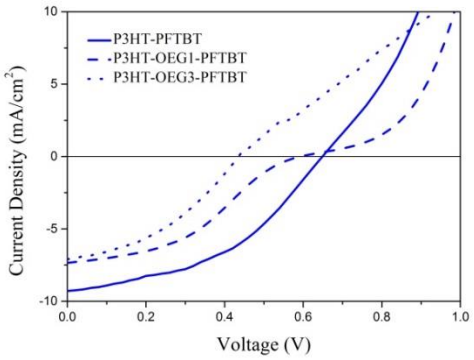

FIGURE 4. Typical J-V curves for ternary blend photovoltaic devices with active layer comprises P3HT-PFTBT P3HT-OEG1-PFTBT, and P3HT-OEG3-PFTBT. Mass ratios for P3HT, PCBM and BCP are fixed at 1:1:0.6

TABLE 2. Device test results for ternary blend OPVs with fixed mass ratios of P3HT, PCBM and BCP or polymer blend at 1:1:0.6 averaged over five devices.

Active Layer	PCE (%)	J_{sc} (mA cm^{-2})	V_{oc} (V)	FF
P3HT-PFTBT Ternary blend	2.49 (±0.05)	8.75 (±0.21)	0.66 (±0.01)	0.43 (±0.01)
P3HT-OEG1-PFTBT Ternary blend	1.29 (±0.13)	6.78 (±0.33)	0.56 (±0.01)	0.29 (±0.03)
P3HT-OEG3-PFTBT Ternary blend	1.14 (±0.06)	7.13 (±0.45)	0.41 (±0.02)	0.39 (±0.01)
P3HT-PFTBT	0.20 (±0.01)	1.08 (±0.03)	0.64 (±0.01)	0.28 (±0.01)
P3HT-OEG1-PFTBT	0.14 (±0.01)	0.80 (±0.03)	0.64 (±0.01)	0.26 (±0.01)
P3HT-OEG3-PFTBT	0.04 (±0.01)	0.40 (±0.02)	0.36 (±0.02)	0.30 (±0.01)

To understand the impact of the linking group structure on photovoltaic device performance, devices with pure BCP active layer and blends of BCP with P3HT and fullerene were fabricated and tested. The characteristics of photovoltaic devices with BCP in the active layer are shown in **Table 2**. The best performance is observed for P3HT-PFTBT material with no linker, but the efficiencies and currents are too low to draw strong conclusions across the series of devices. For further analysis, a series of devices comprised of ternary blends of BCP with P3HT homopolymer and PCBM were fabricated and tested. As shown in **Figure 4**, this series of materials exhibits a similar trend, in which the performance degrades significantly for BCPs with flexible linkers. Dark currents for each device in **Figure 4** are provided in the Supporting Information Figures S25 – 27. We observe a decrease in both the short-circuit current J_{sc} and open-circuit voltage V_{oc}, and the power conversion efficiency PCE as the length of the OEG increases.

The results show a decrease in PCE and V_{oc} after insertion of linking group, which is in agreement with results from PL quenching and shifting. Since donor and acceptor blocks are the same in all BCPs, a decrease in V_{oc} suggests possible formation of energy barriers or of a low energy level charge transfer state induced by linking groups, in which charge transfer in between donor and acceptors is insulated. The induced energy barriers can also lead to a mismatch of the work function between BCPs and charge transport layers, which would account for the kink in the current density vs. voltage curves for P3HT-OEG1-PFTBT and P3HT-OEG3-PFTBT observed in **Figure 4**. We also note that a similar shape in the current-voltage curve has been observed in previous studies of the same or similar donor-acceptor blends, which again suggests a mismatch in the energy levels between donor and acceptor polymers in this system[22,37,38].

Calculations using density functional theory (DFT) at the LC-wPBEh/6-31G(d) level were performed to gain additional insight in energetics, charge transfer, and polymer conformation at the donor and acceptor interface. In this simulation, a model with 12 hexylthiophene repeat units and 3 dioctylfluorene-*co*-benzothiadiazol repeat units was used to simulate the block copolymer P3HT-PFTBT.

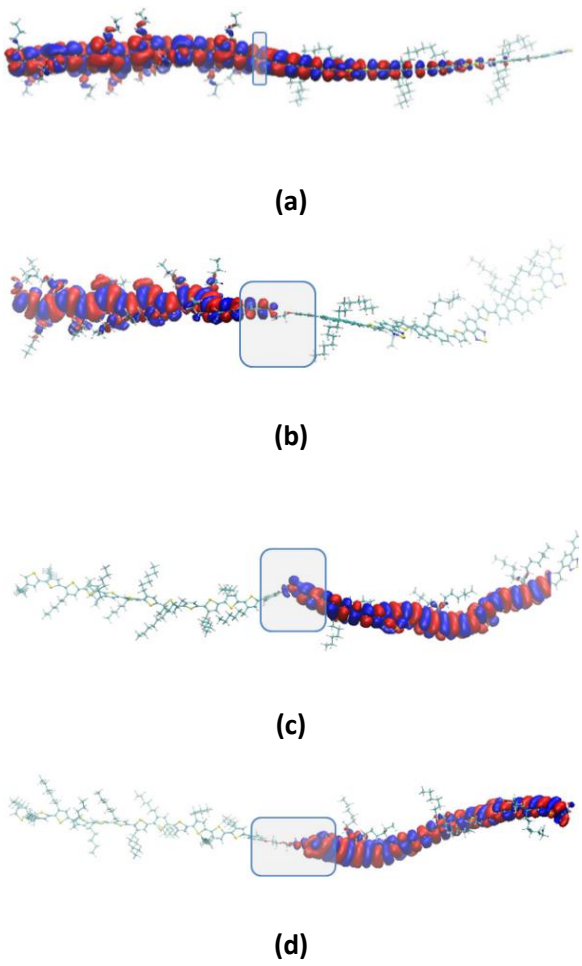

FIGURE 5. Simulated HOMO levels for **(a)** P3HT-PFTBT (planar), **(b)** P3HT-OEG1-PFTBT (planar), **(c)** P3HT-OEG1-PFTBT (non-planar) and **(d)** P3HT-OEG3-PFTBT (non-planar). Linking groups are inside the rectangle region. For all cases, the P3HT fragment is on the left side of the rectangle region (linker) and the PFTBT is on the right side of the rectangle.

In order to analyze the energetics and kinetics of charge and energy transfer at the interface, the conformation of the polymer blocks at the interface was determined through minimization of the conformational free energy followed by analysis of the electronic structure. Optimizations of molecular structures were first performed with semi-empirical PM3 method. Analysis of electronic structure charge transfer rates was performed with LC-wPBEh/6-31G(d). The corresponding HOMO orbitals are shown in **Figure 5 (a, c-d)**. The molecular structure resulting from optimization shows that P3HT and PFTBT blocks both have planar conformations regardless of linker. This is expected, as there is strong π–π conjugation within the P3HT and PFTBT fragments. We also observe that the inter-fragment π–π conjugation persists in the no-linker polymer P3HT-PFTBT. Thus, the structure of P3HT-PFTBT is coplanar with the HOMO strongly delocalized across junction (**Figure 5a**).

As for the molecular structure of BCPs with OEG linker, the OEG fragment is relatively flexible and breaks the inter-fragment π–π conjugations leading to a non-zero dihedral angle between P3HT and PFTBT planes, shown in **Figure 5(c, d)**. To investigate whether interruption of inter-fragment delocalization in the HOMO is caused by the reduced planarity, we performed a constrained planar optimization of P3HT-OEG1-PFTBT in which the dihedral angle between P3HT and PFTBT was manually set to zero. The corresponding planar P3HT-OEG1-PFTBT and its HOMO is shown in **Figure 5(b)** revealing that even when P3HT is oriented in-plane with PFTBT, the π–π conjugation across the junction can still be disrupted and therefore has a strong effect on charge transport across junction.

Overall, the OEG linking group serves as an insulator to reduce overlap of electron density at the donor and acceptor junction. This is clearly seen in the simulated HOMO energy level and the density of states depicted in **Figure 5**. The electron density resides mostly in PFTBT block after insertion of OEG linking group. This is due to the energy barrier induced by OEG linking group and is therefore expected to impede electron transport from P3HT to linker

and hole transport from PFTBT to linker. Electron and hole transfer are still available from donor LUMO+ and acceptor HOMO- energy levels, but a consequence of twisting at the interface is a further reduction of energetic overlap and diminished charge transport between P3HT and PFTBT blocks.

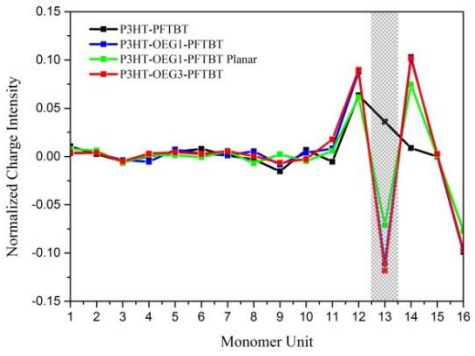

FIGURE 6. Charge distribution along the BCP chain from Mulliken population analysis. The P3HT model consists of 12 monomers numbered from 1 to 12. PFTBT consists of 3 monomers numbered from 14 to 16. The linker is represented by the gray rectangular block (unit 13).

Mulliken population analysis was carried out to further understand the insulation effect of the linking group at the donor and acceptor junction.[39] This method is used to determine partial charge distribution on each monomer unit through linear combination of molecule orbitals. In our analysis, P3HT monomers are numbered from 1-12, the linking group is numbered 13, and PFTBT monomers are numbered from 14-16, as shown in **Figure 6**. At the donor and acceptor interface, insertion of a linking group creates a negative charge space polarization on the linker. P3HT and PFTBT monomer adjacent to the linking group (unit 12 and 14) are both positively charged as a balance to the negatively charged linking group. This suggests that the linker affects transport along the BCP chain by inducing a charge space separation region and a buildup potential, which therefore creates a barrier for electron transfer from donor to the linking group.

To further analyze the effect of the linking group at the donor and acceptor interface, transfer integrals were calculated between donor and linker, and between linker and acceptor.[40] These quantities are described for carrier mobility along the backbone of BCP chain. For example, transfer integrals between HOMOs of the donor-linker-acceptor describe the transport of holes across the BCP junction. Similarly, transfer integrals between LUMOs of donor-linker-acceptor are directly related to transport of electrons across BCP junction. The decomposition of electronic structure on the HOMOs and LUMOs of donor, acceptor and linker for P3HT-PFTBT and P3HT-PFTBT is shown in **Figure S28-30**. As can be seen, linkers significantly block transfer of carrier charges along the BCP chain since their transfer integrals are not aligned with transfer integrals in donor and acceptor. Out of all cases, the effect of blocking is strongest for OEG3 linker, for which coupling between the LUMO of the linker and the LUMO of the acceptor is only 0.02 meV, and coupling between HOMO of donor and HOMO of linker is 1.5 meV. This is expected since a longer length of OEG has a stronger insulation in charge transport. The calculated HOMO and LUMO levels for P3HT, OEG, and PFTBT blocks suggest that the energy level of the linking group is not aligned optimally to facilitate carrier transfer but instead may insulate charge separation and transportation at the donor and acceptor interface.

TABLE 3. Simulated V_{oc}, separation and recombination energy for block copolymers

Active Layer	Separation (meV)	Recombination (meV)	Separation/ Recombination Ratio	Simulated V_{oc} (V)
P3HT-PFTBT	3.5×10^{2}	2.6×10^{1}	13	0.64
P3HT-OEG1-PFTBT	1.1	1.2×10^{-1}	9.0	0.62
P3HT-OEG1-PFTBT (planar)	4.6	2.0	2.3	0.48
P3HT-OEG3-PFTBT	1.6×10^{-3}	9.3×10^{-4}	1.7	0.44

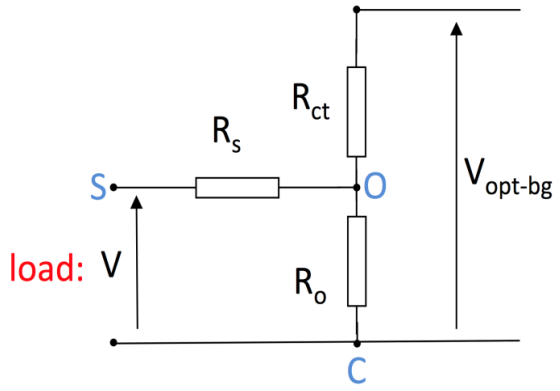

FIGURE 7. Equivalent circuit model for BCP based photovoltaic cell. R_{ct} and R_o represent resistance related to interfacial charge separation and recombination across heterojunction. R_s is a serial resistance due to finite mobilities of carriers during charge duffusion. $V_{opt\text{-}bg}$ is optical band gap and V represents the measured output voltage of device.

The measured output voltage of the device (V) is reduced from the optical band gap (difference between LUMO of acceptor and HOMO of donor) due to a voltage drop resulting from charge transfer resistance (R_{ct}), charge recombination (R_o), and the serial resistance (R_s). They are related to charge separation, charge recombination, and intermolecular transportation respectively. In the case of open circuit, the serial resistance (R_s) is infinite and voltage drop between points S and O is zero. Thus the measured output voltage V is the same as that measured between points O and C. In the equivalent circuit model, the open circuit voltage is therefore given by $V_{OC} = \frac{V_{opt-bg}}{1+R_{ct}/R_o}$. Since R_o and R_{ct} are inversely proportional to interfacial separation and recombination energy, we get the relationship equation which leads to a simulated V_{oc} for those block copolymers shown in **Table 3**. The result suggests that differences in V_{oc} for pure block copolymer as active layer can be explained from the ratio of simulated separation and recombination rates. This is consistent with experimental results in **Table 2**, suggesting that increase in OEG length will lead to a decrease in V_{oc} value.

Block copolymers with no linker exhibited the largest potential, indicating a stronger driving force for both separation and recombination when there is no insulating linker between donor and acceptor blocks. Insertion of a linker and minimization of the block conformation to a non-planar orientation leads to a dramatic reduction in the potentials for both charge

separation and recombination. The potential for recombination is much lower than for charge separation, indicating a potentially favorable effect on overall photovoltaic efficiency. Increasing the linker length dramatically reduces the potential for both separation and recombination, essentially shutting off charge transfer across the interface. Finally, inserting a linker is able to decrease the ratio of charge separation to recombination at D/A interface, and therefore decrease the value of V_{oc}.

CONCLUSIONS

We demonstrated a synthesis method to insert flexible ethylene and triethylene linking groups in between the donor and acceptor block copolymers via GRIM reaction, followed by end group modification, and completed with Suzuki Miyaura polymerization. Compared to prior works, the primary advantage of this synthesis route is the ability to chemically tune the structure at the donor and acceptor junction of conjugated block copolymers. This allows possible investigation in OPV characteristics of different linkers at the donor/acceptor interface.

Analysis of fluorescence data indicates the formation of low energy level charge transfer state at the junction of the donor and acceptor block copolymers caused by OEG. This is also supported by the DFT calculations in that the OEG linking group serves as a strong insulator and can decrease both tunneling and recombination rates between donor and acceptor polymers. The energies of HOMO and LUMO levels of the linking group do not align well with those of the donor and acceptor blocks. In addition, charge transfer in between donor and acceptor blocks is sensitive to the orientation of OEG. For a block copolymer with a longer linking group, the twisting effect at the donor and acceptor interface is expected to further deteriorate OPV performance.

The simulation result of a decrease of V_{oc} with increase OEG length agrees with solar cell device tests. Device testing in ternary blends by mixing the block copolymer with P3HT and PCBM exhibited a decrease in PCE, V_{oc} and J_{sc} with increasing length of linkers, which validates that the insertion of OEG in the block copolymer can impede charge transfer between donor and acceptors.

This work indicates that conjugated block copolymers can serve as a model system for investigating the effect of the donor/acceptor interfacial properties applied to macroscale OPV performance. The capability of linking groups in tuning electrical properties at the D/A interface provides us opportunities to seek linker materials that can improve energy transfer between donor and acceptor blocks. Future optimization in linking chemistry should take both orientation and the charge insulation effect into account.

ACKNOWLEDGEMENTS

We acknowledge the support of the National Science Foundation DMR-1352099 and the Welch Foundation for Chemical Research C-1888. A portion of this research was conducted at the Center for Nanophase Materials Sciences, which is a DOE Office of Science User Facility. This research used resources of the Advanced Photon Source, a U.S. Department of Energy (DOE) Office of Science User Facility operated for the DOE Office of Science by Argonne National Laboratory under Contract No. DE-AC02-06CH11357.

REFERENCES AND NOTES

1. Z. He, C. Zhong, S. Su, M. Xu, D. Wu, Y. Cao, *Nat. Photonics* **2012**, 6, 591–595.

2. B. Kippelen, J.-L. Brédas, *Energy Environ. Sci.* **2009**, 2, 251–261.

3. Y. Zhou, C. Fuentes-Hernandez, J. Shim, J. Meyer, A. J. Giordano, H. Li, P. Winget, T. Papadopoulos, H. Cheun, J. Kim, M. Fenoll, A. Dindar, W. Haske, E. Najafabadi, T.M. Khan, H. Sojoudi, S. Barlow, S. Graham, J. Bredas, S.R. Marder, A. Kahn, B. Kippelen, **2012** *Science* 336, 327–332.

4. S. Berny, N. Bloudin, A. Distler, H. Egelhaaf, M. Krompiec, A. Lohr, O. Lozman, G.E. Morse, L. Nanson, A. Pron, T. Sauermann, N. Seidler, S. Tierney, P. Tiwana, M. Wagner, H. Wilson, *Adv. Sci.* **2016**, 3.

5. S. B. Darling, F. You, *RSC Adv.* **2013**, 3, 17633–17648.

6. S. B. Darling, *Energy Environ. Sci.* **2009**, 2, 1266–1273.

7. A. Yassar, L. Miozzo, R. Gironda, G. Horowitz, *Prog. Polym. Sci.* **2013**, 38, 791–844.

8. T. Smart, H. Lomas, M. Massignani, M.V. Flores-Merina, L.R. Perez, G. Battaglia, *Nano Today* **2008**, 3, 38–46.

9. H.-F. Jiao, X. Wang, K. Yao, P. Chen, Z. Jia, Z. Peng, F. Li, *J. Mater. Chem. B.* **2016**, 4, 7882–7887.

10. M. J. Robb, S.-Y. Ku, C. J. Hawker, *Adv. Mater.* **2013**, 25, 5686–5700.

11. T. M. Clarke, J. R. Durrant, *Chem. Rev.* **2010**, 110, 6736–6767.

12. P. K. Nayak, K. L. Narasimhan, D. Cahen, *J. Phys. Chem. Lett.* **2013**, 4, 1707–1717.

13. P. E. Shaw, A. Ruseckas, I. D. W. Samuel, *Phys. Rev. B* **2008**, 78, 245201.

14. Y. Zhong, A. Tada, S. Izawa, K. Hashimoto, K. Tajima, *Adv. Energy Mater.* **2014**, 4.

15. I. H. Campbell, B. K. Crone, *Appl. Phys. Lett.* **2012**, 101, 023301.

16. S.-J. He, D.-K. Wang, N. Jiang, Z.-H. Lu, *J. Phys. Chem. C.* **2016**, 120, 21325–21329.

17. H. Kuang, M. J. Janik, E. D. Gomez, *J. Polym. Sci. Part B Polym. Phys.* **2015**, 53**,** 1224–1230.

18. Y. Lee, E. Gomez, *Macromolecules.* **2015**, 48, 7385–7395.

19. G. Feng, J. Li, F. J. M. Colberts, M. Li, J. Zhang, F. Yang, Y. Jin, F. Zhang, R. A. J. Janssen, C. Li, W. Li, *J. Am. Chem. Soc.* **2017**, 139, 18647–18656.

20. W. Lai, C. Li, J. Zhang, F. Yang, F. J. M. Colberts, B. Guo, Q. M. Wang, M. Li, A. Zhang, R. A. J. Janssen, M. Zhang, W. Li ,*Chem. Mater.* **2017**, 29, 7073–7077.

21. J. H. Lee, C. G. Park, A. Klm, H. J. Kim, Y. Kim, S. Park, M. J. Cho, D. H. Choi, *ACS Appl. Mater. Interfaces* **2018, DOI:** 10.1021/acsami.8b03580.

22. J. W. Mok, Y-H. Lin, K. G. Yager, A. D. Mohite, W. Nie, S. B. Darling, Y. Lee, E. D. Gomez, D. Gosztola, R. D. Schaller, R. Verduzco, *Adv. Funct. Mater.* **2015**, 25, 5578–5585.

23. S.-S. Sun, C. Zhang, A. Ledbetter, S. Choi, K. Seo, C. E. Bonner, M. Drees, N. S. Sariciftci, *Appl. Phys. Lett.* **2007**, 90, 043117.

24. C. Zhang, S. Choi, J. Haliburton, T. Cleveland, R. Li, S-S. Sun, A. Ledbetter, C. E. Bonner, *Macromolecules* **2006**, 39, 4317–4326.

25. D. H. Lee, J. H. Lee, H. J. Kim, S. Choi, G. E. Park, M. J. Cho, D. H. Choi, *J. Mater. Chem. A* 2017, 5, 9745–9751.

26. Y-K. Han, Y-J. Lee, P. C. Huang, *J. Electrochem. Soc.* **2009**, 156, K37-K43

27. Y.-H. Lin, K. A. Smith, C. N. Kempf, R. Verduzco, *Polym. Chem.* **2012**, 4, 229–232.

28. K. A. Smith, Y-H. Lin, J. W. Mok, K. G. Yager, J. Strzalka, W. Nie, A. D. Mohite, R. Verduzco, *Macromolecules* **2015**, 48, 8346–8353.

29. C. Grieco, M. P. Aplan, A. Rimshaw, Y. Lee, T. P. Le, W. Zhang, Q. Wang, S. T. Milner, E. D. Gomez, J. B. Asbury, *The Journal of Physical Chemistry C* **2016**, 120, 6978–6988.

30. M. Sommer, H. Komber, S. Huettner, P. Kohn, N. C. Greeham, W. T. S. Huck, *Macromolecules* **2012**, 45, 4142–4151.

31. R. Verduzco, I. Botiz, D. L. Pickel, S. M. Kilbey, K. Hong, E. Dimasi, S. B. Darling, *Macromolecules* **2011**, 44, 530–539.

32. H. A. Bronstein, C. K. Luscombe, *J. Am. Chem. Soc.* **2009**, 131, 12894–12895.

33. E. Kaul, V. Senkovskyy, R. Tkachov, V. Bocharova, H. Komber, M. Stamm, A. Kiriy, *Macromolecules* **2010**, 43, 77–81.

34. V. Senkovskyy, M. Sommer, R. Tkachov, H. Komber, W. T. S. Huck, A. Kiriy, *Macromolecules* **2010**, 43, 10157–10161.

35. A. Kiriy, V. Senkovskyy, M. Sommer, *Macromol. Rapid Commun.* **2011**, 32, 1503–1517.

36. N. Doubina, J. L. Jenkins, S. A. Paniagua, K. A. Mazzio, G. A. MacDonald, A. Jen, N. R. Armstrong, S. R. Marder, C. K. Luscombe, *Langmuir* **2012**, 28, 1900–1908.

37. C. Guo, Y-H. Lin, M. D. Witman, K. A. Smith, C. Wang, A. Hexemer, J. Strzalka, E. D. Gomez, R. Verduzco, *Nano Lett.,* **2013**, 13, 2957–2963.

38. C. R. McNeill, A. Abrusci, J. Zaumseil, R. Wilson, M. J. McKiernan, J. H. Burroughes, J. J. M. Halls, N. C. Greenham, R. H. Friend, *Appl. Phys. Lett.* **2007**, 90, 193506.

39. R. S. Mulliken, *J. Chem. Phys.* **1955**, 23, 1833–1840.

40. J.-L. Brédas, D. Beljonne, V. Coropceanu, J. Cornil, *Chem. Rev.* **2004**, 104, 4971–5004.